

First-principles Equations of State and Structures of Liquid Metals in Multi-megabar Conditions

Shuai Zhang^{1,2, a)} and Miguel A. Morales^{1, b)}

¹⁾*Lawrence Livermore National Laboratory, Livermore, California 94550, USA*

²⁾*Present address: Laboratory for Laser Energetics, University of Rochester, Rochester, New York 14623, USA*

Liquid metals at extreme pressures and temperatures are widely interested in the high-pressure community. Based on density functional theory molecular dynamics, we conduct first-principles investigations on the equation of state (EOS) and structures of four metals (Cu, Fe, Pb, and Sn) at 1.5–5 megabar conditions and 5×10^3 – 4×10^4 K. Our first-principles EOS data enable evaluating the performance of four EOS models in predicting Hugoniot densities and temperatures of the four systems. We find the melting temperature of Cu is 1000–2000 K higher and shows a similar Clapeyron slope, in comparison to those of Fe. Our structure, coordination number, and diffusivity analysis indicates all the four liquid metals form similar simple close-packed structures. Our results set theoretical benchmarks for EOS development and structures of metals in their liquid states and under dynamic compression.

LLNL-PROC-783211

I. INTRODUCTION

Metallic liquids widely exist in nature at planetary interiors, such as the outer part of the Earth’s core which is made of iron-rich fluids under multi-megabar (Mbar) pressures and thousands-Kelvin temperatures. Essentially, convection of the conductive fluids has been generating a magnetic field that is crucial to the planet’s habitability. Accurate understandings of the structure, equation of state, and transport properties of the high-pressure liquids are crucial to geophysical modeling of the dynamics and chemistry and deciphering the energy budget, geomagnetism, and formation and evolution of the planet.¹

Liquid forms of matter at extreme conditions are also ubiquitously generated in laboratory during shock experiments. Typically, the temperature-pressure conditions probed in the experiments are along the Rankine-Hugoniot curve², which is much steeper than the melting curve and therefore can easily produce high-pressure liquids.

However, as a result of interplay between complexities in atomistic and electronic structures, the study of high-pressure liquids has posed grand challenges to both theory and experiment³. Over the past few decades, experimental studies have been relying on x-ray/neutron scattering and optical probes combined with static compression techniques, such as those using a high-pressure vessel⁴, a multi-anvil press^{5,6}, or a diamond-anvil cell (DAC)^{7,8}, to measure the structure and properties of liquids under pressure. These experiments, usually performed at up to a few tens gigapascal (GPa) in pressure and a few thousands Kelvin in temperature, have revealed many interesting physics of structural and electronic phase transitions in a wide variety of materials. For example, evidences were found on the existence of liquid-liquid phase

(LLP) transitions in single-element substances of phosphorus⁹, silicon^{10–13}, germanium¹⁴, gallium¹⁵, nitrogen¹⁶, and hydrogen^{17–20} as well as in oxides, molecules, and alloys^{21,22}, and on metallization in liquid selenium, sulfur, iodine, nitrogen, and hydrogen^{16,23,24}.

In recent years, techniques that combine ultra-bright, high-energy x-ray with dynamic compression have been developed in places such as the Matter at Extreme Conditions end station of the Linac Coherent Light Source x-ray free-electron laser²⁵ and the Dynamic Compression Sector at Advanced Photon Source²⁶. These advances have enabled *in situ* structural determination of liquids in laboratory along with equations-of-state measurements for matter at extreme conditions.

Theoretically, a natural way of simulating materials at finite temperatures is by doing molecular dynamics (MD). In these simulations, atoms are treated as particles that interact with potentials in certain forms. The potentials are usually empirical and chosen either in analytic or numerical forms (so called “classical MD”). Classical MD approaches have shown great usefulness in simulating materials in a temporal scale (e.g., nanoseconds) that is close to that experienced by materials in shock compression experiments or during meteorite impacts²⁷. The considerable spacial scale (e.g., millions of atoms) of classical MD simulations provides rich information about the response of materials at high pressure and temperatures.^{28,29} However, due to the temperature and pressure dependence of electronic interaction, accuracy and transferability of the empirical potentials and reliability of the classical MD results are typically questionable.^{30,31} And one has to rely on first-principles MD^{32–35}, such as those based on density functional theory (DFT)^{36–38}, in order to acquire a more precise description of the electronic interaction and properties of materials.

As the state-of-art quantum mechanical approach for condensed matter studies, DFT simplifies the many-body interaction in real materials into a single-particle mean field problem, with an effective potential including an exchange-correlation term that is subject to users’ choices in their calculation. This has enabled accurate simulations to the electronic level that is computationally feasible. DFT-MD has been widely used to set theoretical benchmarks for the equation of state (EOS),

^{a)}Electronic mail: szha@lle.rochester.edu

^{b)}Electronic mail: moralesilva2@llnl.gov

structures, and properties of a wide variety of materials at cold to warm dense conditions^{39–49}, in particular liquids in multi-Mbar conditions. These calculations, in synergy with the ongoing experimental developments, are expected to unveil the extreme physics of the matter and provide important inputs for developing better potentials for large-scale MD simulations and building reliable EOS models for hydrodynamic simulations.

In this paper, we report DFT-MD simulations of four metals: iron (Fe), copper (Cu), lead (Pb), and tin (Sn). The calculations are at 1.5–5 Mbar around the respective Hugoniot curve of the materials. The discussions are focused on the EOS, shock Hugoniot, and the atomistic structure. We also briefly talk about transport properties in connection to the structural results. Our results indicate that all the four systems, when in their liquid form and at the conditions considered in this work, show close-packed simple structures.

II. COMPUTATIONAL DETAILS

All our MD calculations are conducted within DFT and using the Vienna Ab-initio Simulation Package (VASP)⁵⁰. The setup of the simulations are summarized in Table I. For simplicity, we implement the “mean-value” k point⁵¹ of $(1/4, 1/4, 1/4)2\pi/a$, where a denotes the size of the cubic simulation cell, to sample the entire Brillouin zone. We use the Perdew-Burke-Ernzerhof (PBE) exchange-correlation functional, a projected augmented wave (PAW)⁵² pseudopotential, and time steps of 1.5–5.2 fs that depend on the temperature and the density.

For Fe and Cu, we start each simulation from a 128-atoms cell constructed by $4 \times 4 \times 4$ times the 2-atom body-centered-cubic (bcc) unit cell. The simulations of Sn and Pb use cubic cells each containing 256 atoms and starting with representative liquid snapshots from simplified “warm-up” calculations. The setup for the “warm-up” calculations is similar to the main, productive ones but the number of electronic bands are smaller. This makes the calculation faster while still generating reasonable structural snapshots in the number of a few thousands that consist the MD trajectory. The starting configuration for the “warm-up” calculations are $4 \times 4 \times 4$ times the 4-atom face-centered-cubic (fcc) unit cell.

We use a Nosé thermostat⁵³ to generate MD trajectories in canonical (NVT , i.e., constant number of atoms, constant volume, and constant temperature) ensembles. Each MD trajectory consists 12000–20000 steps for Sn and Pb, and 1000–8000 steps for Cu and Fe. When calculating the EOS and analyzing the structures, we disregard the beginning 20% and perform block averaging over the remaining part of each MD trajectory, in order to make sure the analysis are for the system in equilibrium. The ion kinetic contributions to the pressure and energy are included in the EOS following an ideal gas model. We perform convergence tests on the cell size, basis set cutoff, and k sampling point/grid, and found the EOS, structure, and diffusivity results to be the same within the standard errorbar of our data.

Using the EOS data from the DFT-MD calculations, we

determine the pressure-density-temperature shock Hugoniot curves. This is done via the Rankine-Hugoniot equation² $\mathcal{H} = E - E_0 - (P + P_0)(V_0 - V)/2 = 0$, where (E, P, V) and (E_0, P_0, V_0) denote the total internal energy, pressure, and volume of a sample under steady shock and in the initial state, respectively. The Hugoniots that are obtained by first fitting the EOS along each isochore (isochore) using cubic splines and then determining the pressure, energy, and volume (temperature) conditions at which the Hugoniot equation is satisfied. The values for the initial energy and pressure used in this work are summarized in Table II. We obtain these numbers by performing DFT calculations using the ambient structure of each metal, i.e., fcc at 8.96 g/cm³ for Cu, ferromagnetic bcc at 7.877 g/cm³ for Fe, bcc at 11.34 g/cm³ for Pb, and β -tin at 7.287 g/cm³ for Sn. An additional bcc (fcc) structure with the same density for Cu (Pb) was tested to check the dependence of the Hugoniot on the initial condition.

We calculate the radial distribution function $g(r)$ by analyzing inter-atomic distances along MD trajectories. The structure factor is obtained from $g(r)$ according to the definition $S(k) = 1 + 4\pi n \int_0^\infty r^2 \frac{\sin(kr)}{kr} [g(r) - 1] dr$, where n is the density in units of atoms/volume. We choose the number of bins to be ~ 100 when calculating $g(r)$ and a bin size of 0.005 Å⁻¹ when calculating $S(k)$. We have tried other bin sizes and found the $g(r)$ and $S(k)$ profiles are not sensitive to those variations. We also calculate $S(k)$ from the DFT-MD trajectories according to its definition $\langle \rho^*(k)\rho(-k) \rangle$, where $\rho(k) = \int \exp(i\mathbf{k} \cdot \mathbf{r}) d\mathbf{r}$ is the electron density, and found $S(k)$ results obtained in the two separate ways are consistent with each other.

III. RESULTS AND DISCUSSION

A. EOS and Hugoniot

Our first-principles EOS and Hugoniot for the four metals are summarized in Fig. 1. We also show Hugoniots predicted by LEOS models (LEOS 260 for Fe, LEOS 290 for Cu, LEOS 820 for Pb, and LEOS 500 for Sn) to evaluate their performances by comparing to our DFT-MD results.

Our EOS results show that, around 1.5–5.0 Mbar, the Hugoniot temperatures of Pb and Sn is higher than that of Fe and Cu. This is explained by the larger compression ratio of Pb and Sn than Fe and Cu, which has to be compensated by a larger increase in the internal energy according to the Hugoniot equation $E - E_0 = (P + P_0)(V_0 - V)/2$. The larger compression ratio of Pb and Sn is consistent with their smaller bulk moduli⁵⁸ and larger thermal expansion coefficients⁵⁹ than those of Fe and Cu.

Along the isochores, our DFT-MD data show discontinuity in pressure at densities between 12.0–13.5 g/cm³ for Fe and 13.0–15.0 g/cm³ for Cu. This is a signature that the simulation temperature is near the melting curve. We use the mean-square displacement (MSD) as a criteria for judging whether the system remains an equilibrium fluid, a crystalline solid (shown with black symbols in Fig. 1), or some meta-stable (red symbols in Fig. 1) state. This analysis gives melting temperatures of Fe that are consistent with recent experiments⁵⁴.

TABLE I. Parameters chosen in our DFT-MD simulations.

	Fe	Cu	Pb	Sn
atoms/simulation cell	128	128	256	256
E_{cutoff} (eV)	800	800	500	400
ENMAX (eV)	267.882	295.446	97.973	103.236
r_c (Bohr)	2.3	2.3	3.1	3.0
valence electrons	8	11	4	4
Pseudopotential	PAW, 22Jun2005	PAW, 06Sep2000	PAW, 08Apr2002	PAW, 08Apr2002
Exchange-correlation functional	PBE			
k -point	$(1/4, 1/4, 1/4)2\pi/a$ (a being the lattice constant of the cubic simulation cell)			

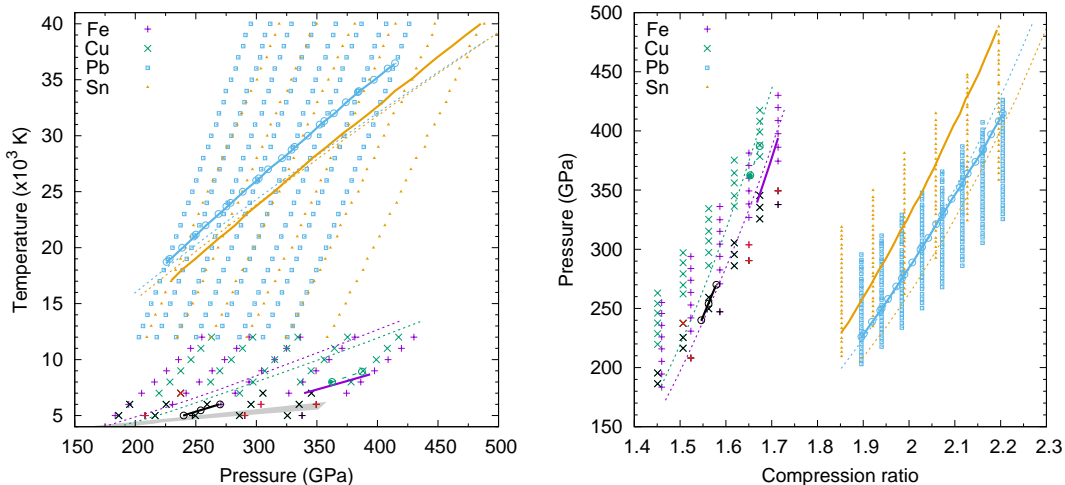


FIG. 1. (left) Temperature-pressure and (right) pressure-compression ratio representation of the equations of state in this study. Symbols denote the EOS data points. Solid and dashed curves are the principle Hugoniot from our first-principles calculations and LEOS models, respectively. Black- and red-colored symbols denote simulations that show solidification and instability features respectively, according to the analysis of the mean-square displacement. The compression ratio is with respect to the ambient density of the corresponding metal, i.e., 7.877 g/cm³ for bcc iron, 8.96 g/cm³ for fcc copper, 11.34 g/cm³ for bcc lead, and 7.287 g/cm³ for β tin. The open circles along the Cu (Pb) Hugoniots are Hugoniot conditions corresponding to a bcc (fcc) initial structure with the same density as that used for the fcc initial structure. The gray shaded area in the left panel denotes the recently measured melting curve of iron in resistance-heated DAC⁵⁴. The shock-wave data for iron melting temperature scatter above the DAC curve by ~ 500 – 1700 K^{55–57}.

TABLE II. Initial conditions determined by DFT calculations and used for constructing Hugoniots in this work.

	Fe	Cu	Cu	Pb	Pb	Sn
	bcc	fcc	bcc	bcc	fcc	β
ρ_0 (g/cm ³)	7.877	8.96	8.96	11.34	11.34	7.287
E_0 (eV/atom)	-8.228	-3.726	-3.688	-3.517	-3.558	-3.785
P_0 (GPa)	-6.60	3.73	0.52	1.91	2.15	2.58

Our results also show the melting temperature of Cu is 1000–2000 K higher than that of Fe in the pressure range of 2–3.75 Mbar. In comparison to the comparison by Japel *et al.*⁶⁰ at up to 1 Mbar, our results indicate the Clapeyron slopes of the melting curves of Fe and Cu become more similar in the regime of 1.75–3.75 Mbar than below 1 Mbar.

In comparison to predictions by the LEOS models, our results indicate that LEOS 290 (260) predicts Cu (Fe) to be slightly harder along the Hugoniot at pressures above 2 Mbar and more so for Cu in the solid regime. On the contrary, LEOS

500 predicts Sn to be softer than our first-principles predictions and LEOS 820 predictions for the pressure-density Hugoniots of Pb are very similar to our DFT-MD results. For the temperature-pressure Hugoniot, the LEOS 500 predictions for Sn are similar to our DFT-MD data, while LEOS 260 (290) predictions for Fe (Cu) are higher and LEOS 820 predictions for Pb are lower by up to 4000 K ($\sim 40\%$ for Fe, $\sim 30\%$ for Cu, $\sim 10\%$ for Pb) in the pressure range of 2–4 Mbar.

The LEOS models are constrained by experimental Hugoniot data (up to 1.5–3.7 Mbar for Fe, Cu, Pb, and Sn)⁶¹ and subject to errors due to the choice in the value of thermodynamic properties (e.g., Debye temperature and Grüneisen parameter) in the models for ion thermal and electron thermal (e.g., Thomas-Fermi or Purgatorio) contributions to the free energy, in particular at pressures where no experiment is available. This could be a major reason for the differences between the Hugoniots predicted by the LEOS models and our calculations. We note that the use of exchange-correlation functional in DFT to approximate the electronic interaction in real materials can also contribute to the differences, because of the non-

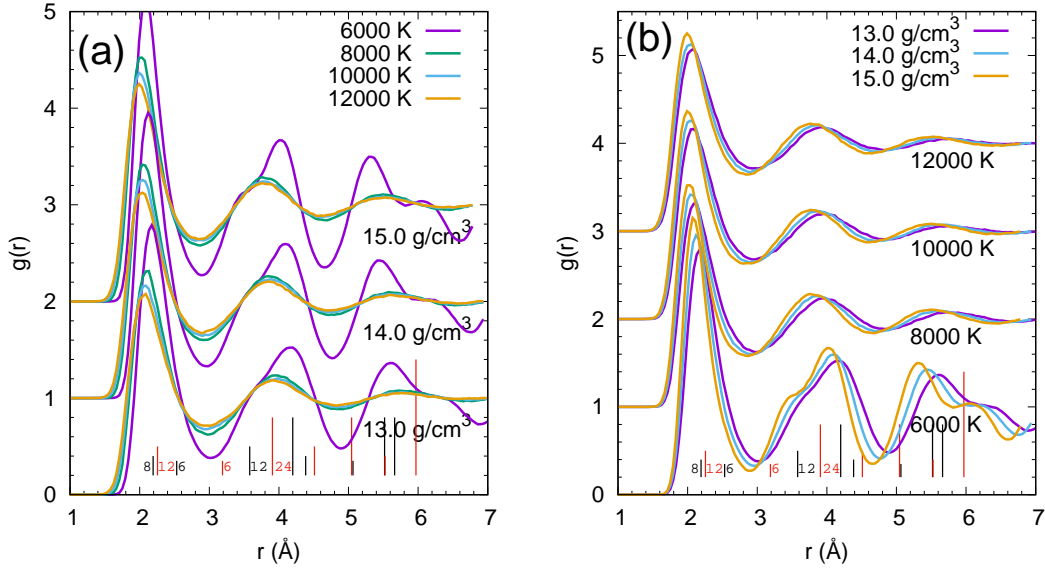


FIG. 2. Pair-correlation function of copper at various temperatures and densities. Different isochores (a) and isotherms (b) have been shifted apart for clarity. Positions of the up-to-eighth (seventh)-nearest-neighbor shells of a perfect body (face)-centered-cubic crystal at 13.0 g/cm^3 are also shown with black (red) vertical bars for comparison. The height of bars are scaled by the coordination number of the corresponding shells, which are labeled for the first few shells.

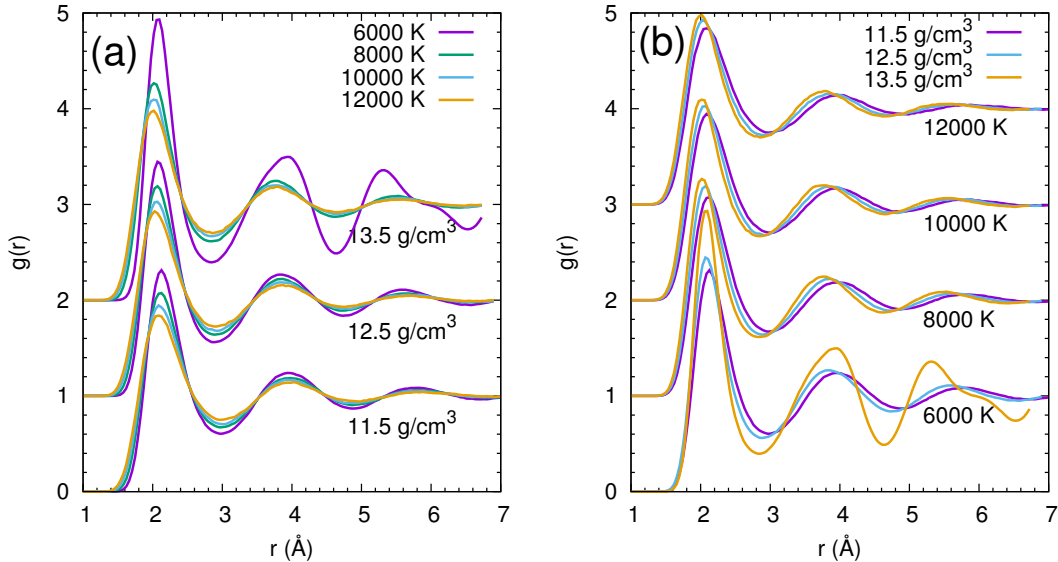


FIG. 3. Pair-correlation function of iron at varies temperatures and densities. Different isochores (a) and isotherms (b) have been shifted apart for clarity.

uniformity of electrons density distribution due to the difference between the more localized inner-shell orbitals and the more extended valence and conduction states. Other factors, such as pseudopotentials and electron relativistic effects may also be critical when considering heavy elements⁶² and high pressures. However, previous work have indicated DFT can predict high-pressure EOS that agree remarkably well with experiments. Examples include Cu under ramp compression to terapascal conditions⁶³ and the ground-state isotherm of a wide variety of materials up to 1 Mbar⁶⁴. The thousands-

Kelvin temperatures being studied are also much higher than the typical Curie temperature of metals, therefore the electron correlation effects could be less a problem than at the ground state. However, detailed discussion on this is beyond the scope of this work and will be addressed, for the case of Sn, in a separate publication⁶⁵.

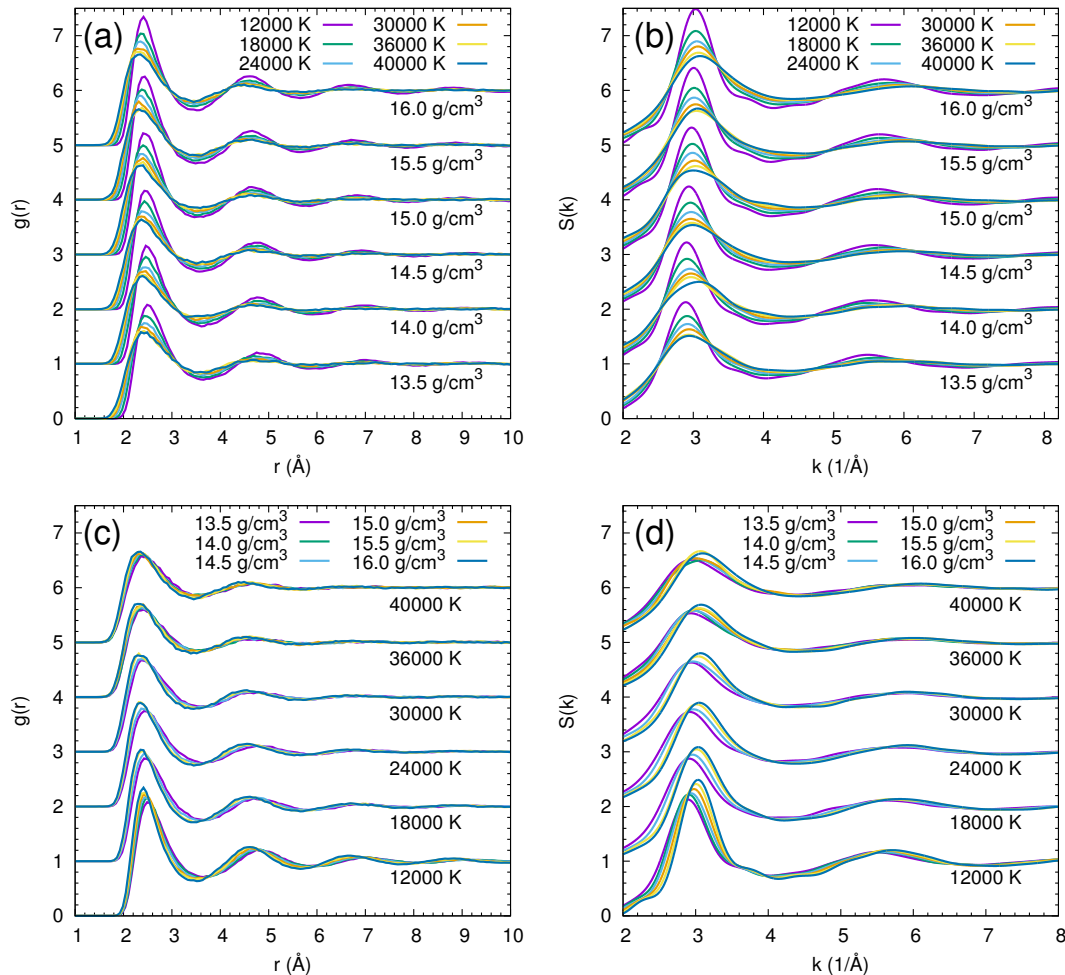


FIG. 4. (left) Pair-correlation function and (right) structure factor of liquid tin at varies temperatures and densities. Different isochores (a-b) and isotherms (c-d) have been shifted apart for clarity.

B. Atomistic structure

We characterize the atomistic structure using the radial distribution function $g(r)$, which reflects the local density changes as a function of the inter-atomic distance. The $g(r)$ profiles of Cu at selected densities and temperatures are summarized in Fig. 2. At 6000 K, the $g(r)$ results show distinct peak-valley structures and long-range correlations, which are typical for a solid at high temperature and is consistent with that expected from a bcc crystal. This provides direct evidence for the stability of solid Cu at these conditions and is consistent with the EOS discontinuity that was discussed in the previous sub-section. Note that Cu in its ground state remains an fcc structure at pressures as high as 10–23 Mbar⁶³, whose melting temperature, if estimated to ~ 200 GPa based on the measurements by Japel *et al.*⁶⁰, is in reasonable consistency with our estimated range (6000–7000 K) for the melting temperature of the bcc structure.

At temperatures of 8000 K or higher, the overall profiles of $g(r)$ are similar among different isochores or isotherms: a primary peak exists at 2 Å, which is followed by a valley at 3 Å,

two additional peaks at 3.8 and 5.6 Å that become weaker at larger distances, and a smoothly flattened tail at 6.2 Å or greater. The primary peak has a height exceeding 2, and it gradually decreases and broadens as temperature increases, or increases and shifts to smaller r as density increases. Coordination analysis of the liquid states indicates a coordination number $CN=4\pi n \int_0^{r_{\text{valley}1}} g(r)r^2 dr=12-14$ for the first shell and the value is not clearly dependent on temperature or density, consistent with that of a simple close-packed liquid structure. Note that we would get $CN=5-7$ if using $8\pi n \int_0^{r_{\text{peak}1}} g(r)r^2 dr$, which indicates that, in liquid Cu, the nearest-neighbor atoms are pushed to larger r and the second-nearest-neighbor atoms are pulled to smaller r relative to those in a bcc solid.

Our $g(r)$ profiles for Fe (Fig. 3) are similar to those of Cu. The results show a bcc solid feature at 6000 K and 13.5 g/cm³ but are simple close-packed liquid structures at all other conditions shown in the diagram.

The Sn and Pb results are shown in Figs. 4 and 5. We also present the structure factor $S(k)$ results for Sn in Fig. 4. Similar to the those of liquid Cu and Fe, the $g(r)$ of Sn and Pb also has a primary peak that corresponds to $CN=12-14$ (when

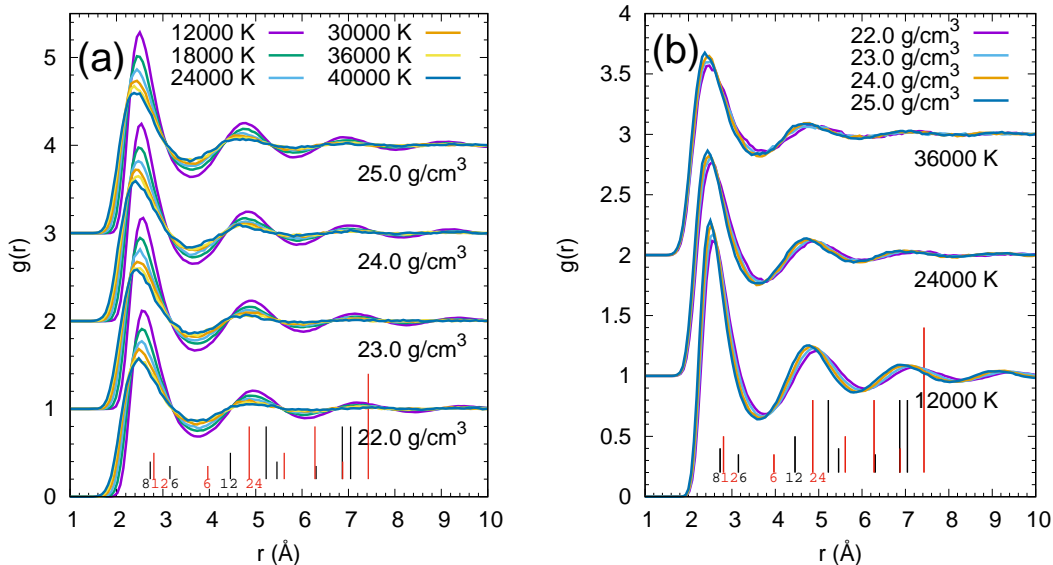


FIG. 5. Pair-correlation function of liquid lead at varies temperatures and densities. Different isochores (a) and isotherms (b) have been shifted apart for clarity. Positions of the up-to-eighth (seventh)-nearest-neighbor shells of a bcc (fcc) crystal at 22.0 g/cm^3 are also shown with black (red) vertical bars for comparison. Notations for the bars are the same as Fig. 2.

integrating to the first valley) and shows similar trends with density and temperature as those of Cu. However, the height of the primary peak gets smaller than 2, because of the high temperatures, and the peak positions look more similar to the neighbor-shell positions of a fcc than bcc solid. It is noteworthy that these are signatures of simple close-packed metallic liquid and do not depend on the initial structure of the simulation cell—we have compared 128- and 256-atom cells for Sn and found the same $g(r)$ profiles. Recent x-ray diffraction measurements of Sn under shock compression to 90 GPa also show liquid structures that are consistent with the DFT-MD predictions⁶⁶.

A tiny bump is observed in Fig. 4 along the $S(k)$ profiles of Sn at 12000 K but not at higher T . This indicates a gradual structural transition in liquid Sn at $T \leq 12000 \text{ K}$. However, we observe no clear difference between the $g(r)$ profiles at 12000 K and those at higher temperatures, nor in the $g(r)$ profiles of liquid Pb at the conditions considered in this study. Whether this is associated with LLP or electronic transition is an interesting question that is beyond the scope of discussion in this work and should be addressed in a future paper.

C. Self diffusivity

A basic transport property of a liquid is the diffusivity. This is usually characterized by the Arrhenius relation $\ln D \propto 1/T$, where D is the self diffusion coefficient and the slop corresponds to an “activation energy” E_a , which indicates the energy barrier associated with the packing efficiency of the first shell of neighboring atoms.

We calculate the self diffusion coefficient D using the Einstein relation $D = \text{MSD}/6\tau$, where τ is the length of the simu-

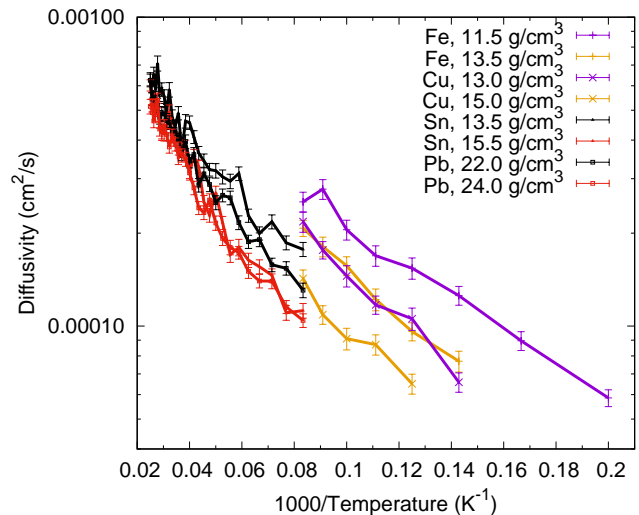


FIG. 6. Arrhenius plot of the self diffusion coefficient for four liquid metals at varies densities.

lation in time, and plot the results for the four metals at representative densities in Fig. 6. Our results show that, for all four metals, diffusion is hindered when density increases or temperature decreases, due to the increased packing or decreased kinetics. The Arrhenius behavior is satisfied for all the four liquid metals at various densities. The slope for the different metals at different densities are similar, indicating similar activation energy E_a and coordination environment. This is consistent with our findings that all four metals in their liquid form have simple close-packed structures, based on the $g(r)$ and CN analysis in the previous sub-section.

IV. CONCLUSION

In this work, we report first-principles equations of state, structures, and transport properties of four metallic systems, Cu, Fe, Sn, and Pb, near the Hugoniot and at 1.5–5 Mbar conditions. The calculations are based on state-of-art quantum molecular dynamics using DFT, which provides an accurate description of the electronic interactions and significant advantageous over classical MD approaches.

Our EOS results allow estimating the melting temperature of bcc-Cu to be 6000–8000 K at 1.5–4 Mbar, similar to that of fcc-Cu estimated based on measurements at ≤ 1 Mbar. The melting temperature of bcc-Fe is ~ 1000 –2000 K lower than that of bcc-Cu and the Clapeyron slopes are similar, at variance with previous observations at pressures lower than 1 Mbar.

Our predictions of the shock Hugoniot benchmark the performance of EOS models for these materials. By comparing our first-principles Hugoniot to predictions of LEOS models, we find the Sn model (LEOS 500) is softer by $\sim 10\%$ but gives reasonable temperature-pressure relation; the Pb model (LEOS 820) gives similar pressure-density relation but the Hugoniot temperature is lower, more so at higher pressures with a maximum of deviation of 10% at 4 Mbar; the Fe model (LEOS 260) and the Cu model (LEOS 290) also give similar pressure-density relations to our first-principles predictions for the liquid, but the Hugoniot temperatures are higher by $\sim 30\%$.

Our structural analysis indicates all the four metals in the liquid state and 1.5–5 Mbar are close-packed simple liquids, as characterized by a maximum peak in $g(r)$ at 2–3 Å that decreases both in distance and height with temperature and decreases in distance but increases in height with density, and correspond to a coordination number of 12–14.

The self diffusion coefficient show good Arrhenius behavior with respect to temperature and indicate similar activation energy among the four different liquid metals, re-affirming that they form simple close-packed structures at the multi-Mbar conditions.

V. APPENDIX

The equation of state data for Fe, Cu, Pb, and Sn at megabar pressures calculated using DFTMD and reported in this manuscript are listed in the Table III.

ACKNOWLEDGMENTS

This work was performed under the auspices of the U.S. Department of Energy by Lawrence Livermore National Laboratory (LLNL) under Contract No. DE-AC52-07NA27344. We acknowledge support from the LLNL Lab Directed Research and Development (LDRD) program 18-ERD-012. Computational support was provided by LLNL high-performance computing facility and the Computational Grand Challenge Award.

This document was prepared as an account of work sponsored by an agency of the United States government. Neither the United States government nor Lawrence Livermore National Security, LLC, nor any of their employees makes any warranty, expressed or implied, or assumes any legal liability or responsibility for the accuracy, completeness, or usefulness of any information, apparatus, product, or process disclosed, or represents that its use would not infringe privately owned rights. Reference herein to any specific commercial product, process, or service by trade name, trademark, manufacturer, or otherwise does not necessarily constitute or imply its endorsement, recommendation, or favoring by the United States government or Lawrence Livermore National Security, LLC. The views and opinions of authors expressed herein do not necessarily state or reflect those of the United States government or Lawrence Livermore National Security, LLC, and shall not be used for advertising or product endorsement purposes.

- ¹P. Olson, in *Treatise on Geophysics*, Vol. 8 (Elsevier, 2007) pp. 1–30.
- ²M. A. Meyers, *Dynamic Behavior of Materials* (Wiley, New York, 1994).
- ³P. F. McMillan, M. Wilson, M. C. Wilding, D. Daisenberger, M. Mezouar, and G. Neville Greaves, *J. Phys.: Condens. Matter* **19**, 415101 (2007).
- ⁴M. Inui, K. Sato, K. Mifune, K. Matsuda, D. Ishikawa, and K. Tamura, *J. Non-Cryst. Solids* **353**, 3371–3375 (2007).
- ⁵K. Tsuji, K. Yaoita, M. Imai, O. Shimomura, T. Kikegawa, and M. Imal, *Rev. Sci. Instrum.* **60**, 34505 (1989).
- ⁶A. Yamada, Y. Wang, T. Inoue, W. Yang, C. Park, T. Yu, and G. Shen, *Rev. Sci. Instrum.* **82**, 015103 (2011).
- ⁷G. Shen, V. B. Prakapenka, M. L. Rivers, and S. R. Sutton, *Phys. Rev. Lett.* **92**, 185701 (2004).
- ⁸J. H. Eggert, G. Weck, P. Loubeyre, and M. Mezouar, *Phys. Rev. B* **65**, 174105 (2002).
- ⁹Y. Katayama, T. Mizutani, W. Utsumi, O. Shimomura, M. Yamakata, and K.-i. Funakoshi, *Nature* **403**, 170–173 (2000).
- ¹⁰S. Sastry and C. Austen Angell, *Nat. Mater.* **2**, 739–743 (2003).
- ¹¹P. F. McMillan, M. Wilson, D. Daisenberger, and D. Machon, *Nat. Mater.* **4**, 680–684 (2005).
- ¹²M. Beye, F. Sorgenfrei, W. F. Schlotter, W. Wurth, and A. Fohlisch, *Proc. Natl. Acad. Sci.* **107**, 16772–16776 (2010).
- ¹³V. V. Vasisht and S. Sastry, in *Liquid Polymorphism*, Vol. 152 (John Wiley & Sons, Inc., 2013) Chap. 18, pp. 463–517.
- ¹⁴M. H. Bhat, V. Molinero, E. Soignard, V. C. Solomon, S. Sastry, J. L. Yarger, and C. A. Angell, *Nature* **448**, 787–790 (2007).
- ¹⁵C. Tien, E. V. Charnaya, W. Wang, Y. A. Kumzerov, and D. Michel, *Phys. Rev. B* **74**, 024116 (2006).
- ¹⁶S. Jiang, N. Holtgrewe, S. S. Lobanov, F. Su, M. F. Mahmood, R. S. McWilliams, and A. F. Goncharov, *Nat. Commun.* **9**, 2624 (2018).
- ¹⁷V. Dzyabura, M. Zaghoo, and I. F. Silvera, *Proc. Natl. Acad. Sci.* **110**, 8040–8044 (2013).
- ¹⁸R. S. McWilliams, D. A. Dalton, M. F. Mahmood, and A. F. Goncharov, *Phys. Rev. Lett.* **116**, 255501 (2016).
- ¹⁹K. Ohta, K. Ichimaru, M. Einaga, S. Kawaguchi, K. Shimizu, T. Matsuoka, N. Hirao, and Y. Ohishi, *Sci. Rep.* **5**, 16560 (2015).
- ²⁰M. Zaghoo, A. Salamat, and I. F. Silvera, *Phys. Rev. B* **93**, 155128 (2016).
- ²¹V. V. Brazhkin and A. G. Lyapin, *J. Phys.: Condens. Matter* **15**, 6059–6084 (2003).
- ²²M. Kobayashi and H. Tanaka, *Nat. Commun.* **7**, 13438 (2016).
- ²³S. T. Weir, A. C. Mitchell, and W. J. Nellis, *Phys. Rev. Lett.* **76**, 1860–1863 (1996).
- ²⁴V. V. Brazhkin, R. N. Voloshin, S. V. Popova, and A. G. Umnov, *High Press. Res.* **10**, 454–456 (1992).
- ²⁵M. G. Gorman, A. L. Coleman, R. Briggs, R. S. McWilliams, D. McGonegle, C. A. Bolme, A. E. Gleason, E. Galtier, H. J. Lee, E. Granados, M. Sliwa, C. Sanloup, S. Rothman, D. E. Fratanduono, R. F. Smith, G. W. Collins, J. H. Eggert, J. S. Wark, and M. I. McMahon, *Sci. Rep.* **8**, 16927 (2018).

- ²⁶X. Wang, P. Rigg, J. Sethian, N. Sinclair, N. Weir, B. Williams, J. Zhang, J. Hawreliak, Y. Toyoda, Y. Gupta, Y. Li, D. Broege, J. Bromage, R. Earley, D. Guy, and J. Zuegel, *Rev. Sci. Instrum.* **90**, 053901 (2019).
- ²⁷H. J. Melosh, *Meteorit. Planet. Sci.* **42**, 2079–2098 (2007).
- ²⁸A. V. Bolesta and V. M. Fomin, in *AIP Conf. Proc.*, Vol. 1893 (2017) p. 020008.
- ²⁹D. A. Carvajal Jara, M. Fontana Michelon, A. Antonelli, and M. de Koning, *J. Chem. Phys.* **130**, 221101 (2009).
- ³⁰J. N. Glosli and F. H. Ree, *Phys. Rev. Lett.* **82**, 4659–4662 (1999).
- ³¹C. J. Wu, J. N. Glosli, G. Galli, and F. H. Ree, *Phys. Rev. Lett.* **89**, 135701 (2002).
- ³²P. Ganesh and M. Widom, *Phys. Rev. Lett.* **102**, 075701 (2009).
- ³³B. Boates and S. A. Bonev, *Phys. Rev. Lett.* **102**, 015701 (2009).
- ³⁴M. A. Morales, C. Pierleoni, E. Schwegler, and D. M. Ceperley, *Proc. Natl. Acad. Sci.* **107**, 12799–12803 (2010).
- ³⁵C. Pierleoni, M. A. Morales, G. Rillo, M. Holzmann, and D. M. Ceperley, *Proc. Natl. Acad. Sci.* **113**, 4953–4957 (2016).
- ³⁶W. Kohn and L. J. Sham, *Phys. Rev.* **140**, A1133–A1138 (1965).
- ³⁷P. Hohenberg and W. Kohn, *Phys. Rev.* **136**, B864–B871 (1964).
- ³⁸N. D. Mermin, *Phys. Rev.* **137**, A1441–A1443 (1965).
- ³⁹M. A. Morales, S. Hamel, K. Caspersen, and E. Schwegler, *Phys. Rev. B* **87**, 174105 (2013).
- ⁴⁰B. Militzer and S. Zhang, in *AIP Conf. Proc.*, Vol. 1979 (2018) p. 050012.
- ⁴¹S. Zhang, S. Cottaar, T. Liu, S. Stackhouse, and B. Militzer, *Earth Planet. Sci. Lett.* **434**, 264 – 273 (2016).
- ⁴²S. Zhang, K. P. Driver, F. Soubiran, and B. Militzer, *High Energ. Dens. Phys.* **21**, 16–19 (2016).
- ⁴³S. Zhang, K. P. Driver, F. Soubiran, and B. Militzer, *J. Chem. Phys.* **146**, 074505 (2017).
- ⁴⁴S. Zhang, K. P. Driver, F. Soubiran, and B. Militzer, *Phys. Rev. E* **96**, 013204 (2017).
- ⁴⁵S. Zhang, B. Militzer, L. X. Benedict, F. Soubiran, P. A. Sterne, and K. P. Driver, *J. Chem. Phys.* **148**, 102318 (2018).
- ⁴⁶S. Zhang, B. Militzer, M. C. Gregor, K. Caspersen, L. H. Yang, J. Gaffney, T. Ogitsu, D. Swift, A. Lazicki, D. Erskine, R. A. London, P. M. Celliers, J. Nilsen, P. A. Sterne, and H. D. Whitley, *Phys. Rev. E* **98**, 023205 (2018).
- ⁴⁷S. Zhang, A. Lazicki, B. Militzer, L. H. Yang, K. Caspersen, J. A. Gaffney, M. W. Däne, J. E. Pask, W. R. Johnson, A. Sharma, P. Suryanarayana, D. D. Johnson, A. V. Smirnov, P. A. Sterne, D. Erskine, R. A. London, F. Coppari, D. Swift, J. Nilsen, A. J. Nelson, and H. D. Whitley, *Phys. Rev. B* **99**, 165103 (2019).
- ⁴⁸M. Li, S. Zhang, H. Zhang, G. Zhang, F. Wang, J. Zhao, C. Sun, and R. Jeanloz, *Phys. Rev. Lett.* **120**, 215703 (2018).
- ⁴⁹M. Millot, S. Zhang, D. E. Fratanduono, F. Coppari, S. Hamel, B. Militzer, D. Simonova, S. Shcheka, N. Dubrovinskaia, L. Dubrovinsky, and J. H. Eggert, *Geophys. Res. Lett.* (2020), 10.1029/2019GL085476.
- ⁵⁰G. Kresse and J. Furthmüller, *Phys. Rev. B* **54**, 11169 (1996).
- ⁵¹A. Baldereschi, *Phys. Rev. B* **7**, 5212–5215 (1973).
- ⁵²P. E. Blöchl, O. Jepsen, and O. K. Andersen, *Phys. Rev. B* **49**, 16223–16233 (1994).
- ⁵³S. Nosé, *J. Chem. Phys.* **81**, 511–519 (1984).
- ⁵⁴R. Sinmyo, K. Hirose, and Y. Ohishi, *Earth Planet. Sci. Lett.* **510**, 45–52 (2019).
- ⁵⁵J. M. Brown and R. G. McQueen, *J. Geophys. Res. Solid Earth* **91**, 7485–7494 (1986).
- ⁵⁶C. S. Yoo, N. C. Holmes, M. Ross, D. J. Webb, and C. Pike, *Phys. Rev. Lett.* **70**, 3931–3934 (1993).
- ⁵⁷J. H. Nguyen and N. C. Holmes, *Nature* **427**, 339–342 (2004).
- ⁵⁸<https://periodictable.com/Properties/A/BulkModulus.v.html>.
- ⁵⁹<https://periodictable.com/Properties/A/ThermalExpansion.html>.
- ⁶⁰S. Japel, B. Schwager, R. Boehler, and M. Ross, *Phys. Rev. Lett.* **95**, 167801 (2005).
- ⁶¹S. P. Marsh, *LASL Shock Hugoniot Data* (University of California Press, Berkeley, 1980).
- ⁶²R. Ahuja, A. Blomqvist, P. Larsson, P. Pyykkö, and P. Zaleski-Ejgierd, *Phys. Rev. Lett.* **106**, 018301 (2011).
- ⁶³D. E. Fratanduono, R. F. Smith, S. J. Ali, D. G. Braun, A. Fernandez-Pañella, S. Zhang, R. G. Kraus, F. Coppari, J. M. McNaney, M. C. Marshall, L. E. Kirch, D. C. Swift, M. Millot, J. K. Wicks, and J. H. Eggert, *Phys. Rev. Lett.* **124**, 015701 (2020).
- ⁶⁴P. Söderlind, D. Young, P. Söderlind, and D. A. Young, *Computation* **6**, 13 (2018).
- ⁶⁵S. Zhang and M. Morales, in preparation.
- ⁶⁶R. Briggs, M. G. Gorman, S. Zhang, D. McGonegle, A. L. Coleman, F. Coppari, M. A. Morales-Silva, R. F. Smith, J. K. Wicks, C. A. Bolme, A. E. Gleason, E. Cunningham, H. J. Lee, B. Nagler, M. I. McMahon, J. H. Eggert, and D. E. Fratanduono, *Appl. Phys. Lett.* **115**, 264101 (2019).

TABLE III: Equations of state for four metals at megabar pressures calculated using DFTMD. The data include density (ρ), temperature (T), internal energy (E) and its standard error (E_{error}), pressure (P) and its standard error (P_{error}), and a description with metal type and state [liquid (liq.), solid (sol.), or unstable (sol*)]

ρ (g/cm ³)	T (K)	E (eV/atom)	E_{error} (eV/atom)	P (GPa)	P_{error} (GPa)	note
11.50	5000.00	-5.329891	0.002587	183.4108	0.0884	Fe, liq.
11.50	6000.00	-4.920986	0.003193	194.5701	0.1088	Fe, liq.
11.50	7000.00	-4.515845	0.005111	205.2158	0.2033	Fe, liq.
11.50	8000.00	-4.103636	0.004204	215.7905	0.1613	Fe, liq.
11.50	9000.00	-3.701556	0.003636	225.8689	0.1605	Fe, liq.
11.50	10000.00	-3.298742	0.005060	235.6782	0.1913	Fe, liq.
11.50	11000.00	-2.883125	0.006070	245.7125	0.2170	Fe, liq.
11.50	12000.00	-2.481925	0.007336	254.9459	0.3142	Fe, liq.
12.00	6000.00	-4.621283	0.005232	230.8065	0.1959	Fe, liq.
12.00	7000.00	-4.207331	0.005723	242.0172	0.2255	Fe, liq.
12.00	8000.00	-3.795274	0.003834	252.8390	0.1497	Fe, liq.
12.00	9000.00	-3.381674	0.004511	263.4879	0.1996	Fe, liq.
12.00	10000.00	-2.970353	0.005461	273.8140	0.2080	Fe, liq.
12.00	11000.00	-2.564701	0.007380	283.7254	0.2975	Fe, liq.
12.00	12000.00	-2.146736	0.004791	293.9316	0.2175	Fe, liq.
12.50	6000.00	-4.278268	0.004147	270.7420	0.1714	Fe, liq.
12.50	7000.00	-3.851087	0.003717	282.5037	0.1414	Fe, liq.
12.50	8000.00	-3.429263	0.003986	293.9237	0.1489	Fe, liq.
12.50	9000.00	-3.027538	0.004318	304.3220	0.1791	Fe, liq.

continued ...

... continued

ρ (g/cm ³)	T (K)	E (eV/atom)	E_{error} (eV/atom)	P (GPa)	P_{error} (GPa)	note
12.50	10000.00	-2.609267	0.004354	315.1017	0.1528	Fe, liq.
12.50	11000.00	-2.209792	0.006523	324.9948	0.2362	Fe, liq.
12.50	12000.00	-1.772056	0.006011	336.1317	0.2284	Fe, liq.
13.00	7000.00	-3.446895	0.006202	326.8339	0.2208	Fe, liq.
13.00	8000.00	-3.027860	0.004445	338.2889	0.1530	Fe, liq.
13.00	9000.00	-2.612184	0.004794	349.2825	0.1808	Fe, liq.
13.00	10000.00	-2.197207	0.006100	360.0585	0.2116	Fe, liq.
13.00	11000.00	-1.784707	0.008972	370.7469	0.3188	Fe, liq.
13.00	12000.00	-1.363271	0.008094	381.3199	0.3078	Fe, liq.
13.50	7000.00	-3.014449	0.004688	374.5179	0.1422	Fe, liq.
13.50	8000.00	-2.587004	0.004704	386.2468	0.1585	Fe, liq.
13.50	9000.00	-2.163159	0.004989	397.6389	0.1818	Fe, liq.
13.50	10000.00	-1.741604	0.005778	408.7730	0.1728	Fe, liq.
13.50	11000.00	-1.322616	0.005352	419.7924	0.1904	Fe, liq.
13.50	12000.00	-0.910728	0.009000	430.1242	0.3318	Fe, liq.
13.00	7000.00	-0.094671	0.005753	219.5882	0.2648	Cu, liq.
13.00	8000.00	0.250756	0.004860	228.5770	0.2256	Cu, liq.
13.00	9000.00	0.604556	0.011443	237.6012	0.5142	Cu, liq.
13.00	10000.00	0.953658	0.007691	246.0420	0.3147	Cu, liq.
13.00	11000.00	1.308474	0.011894	254.1927	0.5089	Cu, liq.
13.00	12000.00	1.678023	0.010215	262.9623	0.4646	Cu, liq.
13.50	8000.00	0.593897	0.007870	262.2252	0.3600	Cu, liq.
13.50	9000.00	0.907804	0.011270	269.7825	0.4953	Cu, liq.
13.50	10000.00	1.275812	0.009172	279.2658	0.4176	Cu, liq.
13.50	11000.00	1.643082	0.007316	288.5774	0.3325	Cu, liq.
13.50	12000.00	2.006104	0.007170	297.0766	0.3059	Cu, liq.
14.00	7000.00	0.555745	0.012347	286.2523	0.5951	Cu, liq.
14.00	8000.00	0.931516	0.008220	297.2385	0.3800	Cu, liq.
14.00	9000.00	1.287103	0.006000	306.9231	0.2912	Cu, liq.
14.00	10000.00	1.619758	0.006150	315.1948	0.2592	Cu, liq.
14.00	11000.00	1.994450	0.004867	325.1881	0.2511	Cu, liq.
14.00	12000.00	2.362595	0.008414	334.3163	0.3084	Cu, liq.
14.50	8000.00	1.323379	0.006499	336.3662	0.2654	Cu, liq.
14.50	9000.00	1.652881	0.009508	345.2224	0.4266	Cu, liq.
14.50	10000.00	2.033146	0.008177	356.0007	0.3656	Cu, liq.
14.50	11000.00	2.369111	0.014834	364.4996	0.7063	Cu, liq.
14.50	12000.00	2.767980	0.014097	375.3226	0.5558	Cu, liq.
15.00	8000.00	1.737100	0.009891	378.2839	0.4569	Cu, liq.
15.00	9000.00	2.079838	0.008010	388.0854	0.3715	Cu, liq.
15.00	10000.00	2.461830	0.008849	399.1470	0.4100	Cu, liq.
15.00	11000.00	2.808712	0.012853	408.1596	0.5929	Cu, liq.
15.00	12000.00	3.162047	0.007711	417.4906	0.3758	Cu, liq.
21.50	12000.00	4.257651	0.006685	202.9974	0.1381	Pb, liq.
21.50	13000.00	4.593085	0.005323	206.4020	0.1151	Pb, liq.
21.50	14000.00	4.945054	0.005929	209.9948	0.1205	Pb, liq.
21.50	15000.00	5.285054	0.009325	213.1366	0.1966	Pb, liq.
21.50	16000.00	5.660475	0.006324	216.8797	0.1307	Pb, liq.
21.50	17000.00	6.029187	0.010200	220.2663	0.2099	Pb, liq.
21.50	18000.00	6.401480	0.009620	223.5672	0.1963	Pb, liq.
21.50	19000.00	6.784173	0.011451	226.8480	0.2311	Pb, liq.
21.50	20000.00	7.206125	0.012264	230.7629	0.2415	Pb, liq.
21.50	21000.00	7.591985	0.014902	233.8311	0.3090	Pb, liq.
21.50	22000.00	8.016126	0.014176	237.4104	0.2885	Pb, liq.
21.50	23000.00	8.427134	0.013593	240.5180	0.2667	Pb, liq.
21.50	24000.00	8.858081	0.016250	243.8413	0.3218	Pb, liq.
21.50	25000.00	9.296254	0.015371	247.1688	0.2807	Pb, liq.
21.50	26000.00	9.735717	0.014271	250.3447	0.2676	Pb, liq.
21.50	27000.00	10.188634	0.017904	253.5865	0.3391	Pb, liq.
21.50	28000.00	10.617116	0.017677	256.1325	0.3464	Pb, liq.
21.50	29000.00	11.135861	0.011727	260.2429	0.2414	Pb, liq.

continued ...

... continued

ρ (g/cm ³)	T (K)	E (eV/atom)	E_{error} (eV/atom)	P (GPa)	P_{error} (GPa)	note
21.50	30000.00	11.575125	0.022351	262.7635	0.3809	Pb, liq.
21.50	31000.00	12.111450	0.021588	266.8734	0.3819	Pb, liq.
21.50	32000.00	12.559619	0.014196	269.1354	0.2701	Pb, liq.
21.50	33000.00	13.095212	0.031285	272.9958	0.5719	Pb, liq.
21.50	34000.00	13.534431	0.036653	274.7562	0.6554	Pb, liq.
21.50	35000.00	14.121419	0.026019	279.1447	0.4353	Pb, liq.
21.50	36000.00	14.691167	0.014942	282.9355	0.2412	Pb, liq.
21.50	37000.00	15.173474	0.020574	285.0601	0.3205	Pb, liq.
21.50	38000.00	15.755867	0.022269	289.1426	0.4191	Pb, liq.
21.50	39000.00	16.244750	0.031502	290.9869	0.5099	Pb, liq.
21.50	40000.00	16.865688	0.037695	295.5124	0.6132	Pb, liq.
22.00	12000.00	4.611033	0.009053	217.7433	0.1926	Pb, liq.
22.00	13000.00	4.978210	0.011388	221.8917	0.2391	Pb, liq.
22.00	14000.00	5.318470	0.006679	225.2655	0.1482	Pb, liq.
22.00	15000.00	5.680725	0.005907	228.9417	0.1195	Pb, liq.
22.00	16000.00	6.053077	0.007369	232.6261	0.1521	Pb, liq.
22.00	17000.00	6.415140	0.010300	235.9268	0.2134	Pb, liq.
22.00	18000.00	6.783079	0.006243	239.1802	0.1449	Pb, liq.
22.00	19000.00	7.167708	0.016128	242.5790	0.3350	Pb, liq.
22.00	20000.00	7.586762	0.010802	246.4759	0.2123	Pb, liq.
22.00	21000.00	7.968525	0.015040	249.4381	0.3062	Pb, liq.
22.00	22000.00	8.383054	0.017405	252.8915	0.3474	Pb, liq.
22.00	23000.00	8.861280	0.014526	257.4086	0.2816	Pb, liq.
22.00	24000.00	9.204072	0.015281	259.0350	0.2979	Pb, liq.
22.00	25000.00	9.673726	0.013113	262.9418	0.2562	Pb, liq.
22.00	26000.00	10.069328	0.014764	265.2739	0.2629	Pb, liq.
22.00	27000.00	10.573473	0.026614	269.6616	0.5228	Pb, liq.
22.00	28000.00	11.029983	0.022702	272.7825	0.4140	Pb, liq.
22.00	29000.00	11.517111	0.018485	276.4197	0.3382	Pb, liq.
22.00	30000.00	11.987782	0.020226	279.3949	0.3193	Pb, liq.
22.00	31000.00	12.487005	0.030453	282.8386	0.5397	Pb, liq.
22.00	32000.00	13.005971	0.017042	286.6330	0.3123	Pb, liq.
22.00	33000.00	13.537500	0.023877	290.2181	0.4339	Pb, liq.
22.00	34000.00	13.966346	0.034062	292.0267	0.6287	Pb, liq.
22.00	35000.00	14.534687	0.029837	296.1972	0.5384	Pb, liq.
22.00	36000.00	15.103571	0.018071	299.9891	0.3192	Pb, liq.
22.00	37000.00	15.625405	0.032393	303.0878	0.5997	Pb, liq.
22.00	38000.00	16.105066	0.041879	304.9725	0.6976	Pb, liq.
22.00	39000.00	16.596029	0.033239	307.1166	0.6096	Pb, liq.
22.00	40000.00	17.224267	0.031250	311.4705	0.4517	Pb, liq.
22.50	12000.00	5.006481	0.010033	233.8160	0.2146	Pb, liq.
22.50	13000.00	5.358934	0.004834	237.6836	0.1053	Pb, liq.
22.50	14000.00	5.727071	0.009091	241.7219	0.1994	Pb, liq.
22.50	15000.00	6.073118	0.007303	245.0803	0.1567	Pb, liq.
22.50	16000.00	6.435943	0.007845	248.6721	0.1631	Pb, liq.
22.50	17000.00	6.816889	0.011017	252.3922	0.2195	Pb, liq.
22.50	18000.00	7.212443	0.009612	256.2041	0.2135	Pb, liq.
22.50	19000.00	7.590197	0.011030	259.4787	0.2255	Pb, liq.
22.50	20000.00	7.999462	0.011043	263.2201	0.2216	Pb, liq.
22.50	21000.00	8.367667	0.013200	266.0041	0.2820	Pb, liq.
22.50	22000.00	8.760112	0.010412	269.0053	0.2191	Pb, liq.
22.50	23000.00	9.212213	0.017192	273.0462	0.3505	Pb, liq.
22.50	24000.00	9.641598	0.015722	276.4077	0.3094	Pb, liq.
22.50	25000.00	10.094143	0.021065	280.0975	0.4153	Pb, liq.
22.50	26000.00	10.532394	0.013607	283.2828	0.2493	Pb, liq.
22.50	27000.00	11.018215	0.022790	287.1011	0.4301	Pb, liq.
22.50	28000.00	11.408367	0.015986	289.1972	0.3036	Pb, liq.
22.50	29000.00	11.942074	0.024099	293.6437	0.4643	Pb, liq.
22.50	30000.00	12.361293	0.021590	295.8724	0.4140	Pb, liq.
22.50	31000.00	12.838036	0.018176	298.9626	0.3371	Pb, liq.

continued ...

... continued

ρ (g/cm ³)	T (K)	E (eV/atom)	E_{error} (eV/atom)	P (GPa)	P_{error} (GPa)	note
22.50	32000.00	13.472163	0.024795	304.5149	0.4305	Pb, liq.
22.50	33000.00	13.890761	0.023800	306.3293	0.3991	Pb, liq.
22.50	34000.00	14.433232	0.030327	310.1224	0.5748	Pb, liq.
22.50	35000.00	14.916572	0.036915	312.7340	0.6825	Pb, liq.
22.50	36000.00	15.404848	0.024736	315.1531	0.4267	Pb, liq.
22.50	37000.00	16.000122	0.042736	319.5569	0.7313	Pb, liq.
22.50	38000.00	16.547979	0.027121	322.7578	0.4654	Pb, liq.
22.50	39000.00	17.054990	0.053969	325.2672	0.8815	Pb, liq.
22.50	40000.00	17.639297	0.049391	329.0298	0.8247	Pb, liq.
23.00	12000.00	5.398889	0.007668	250.2825	0.1693	Pb, liq.
23.00	13000.00	5.771459	0.008180	254.6444	0.1748	Pb, liq.
23.00	14000.00	6.113699	0.010408	258.1522	0.2249	Pb, liq.
23.00	15000.00	6.478070	0.009076	261.9664	0.2011	Pb, liq.
23.00	16000.00	6.883011	0.010785	266.4058	0.2361	Pb, liq.
23.00	17000.00	7.208523	0.009921	269.0117	0.2127	Pb, liq.
23.00	18000.00	7.605003	0.014604	272.9327	0.3070	Pb, liq.
23.00	19000.00	8.009378	0.014481	276.7311	0.2931	Pb, liq.
23.00	20000.00	8.372145	0.018067	279.5946	0.3853	Pb, liq.
23.00	21000.00	8.811422	0.014834	283.7417	0.2960	Pb, liq.
23.00	22000.00	9.222150	0.010855	287.2735	0.2074	Pb, liq.
23.00	23000.00	9.660186	0.015945	291.0011	0.3206	Pb, liq.
23.00	24000.00	10.095103	0.025938	294.5880	0.5160	Pb, liq.
23.00	25000.00	10.492560	0.011397	297.1618	0.2385	Pb, liq.
23.00	26000.00	10.980228	0.013069	301.3481	0.2724	Pb, liq.
23.00	27000.00	11.400238	0.012154	304.0059	0.2385	Pb, liq.
23.00	28000.00	11.849102	0.031724	307.1553	0.6097	Pb, liq.
23.00	29000.00	12.386978	0.026667	311.8047	0.4909	Pb, liq.
23.00	30000.00	12.834747	0.026109	314.4806	0.5123	Pb, liq.
23.00	31000.00	13.331368	0.030306	317.9744	0.5252	Pb, liq.
23.00	32000.00	13.811607	0.029431	321.0224	0.5352	Pb, liq.
23.00	33000.00	14.346605	0.021720	324.6748	0.4092	Pb, liq.
23.00	34000.00	14.883307	0.048249	328.3880	0.8764	Pb, liq.
23.00	35000.00	15.402465	0.027038	331.7019	0.4878	Pb, liq.
23.00	36000.00	15.947679	0.018469	335.2384	0.3709	Pb, liq.
23.00	37000.00	16.418044	0.034460	337.4895	0.6233	Pb, liq.
23.00	38000.00	17.050227	0.031156	342.1625	0.5614	Pb, liq.
23.00	39000.00	17.591484	0.041252	345.1954	0.6635	Pb, liq.
23.00	40000.00	18.093782	0.038055	347.7126	0.7025	Pb, liq.
23.50	12000.00	5.832144	0.005531	268.0944	0.1254	Pb, liq.
23.50	13000.00	6.180798	0.006871	271.9304	0.1588	Pb, liq.
23.50	14000.00	6.538166	0.008161	275.8477	0.1774	Pb, liq.
23.50	15000.00	6.909544	0.007755	279.7826	0.1725	Pb, liq.
23.50	16000.00	7.290022	0.009572	283.8429	0.1983	Pb, liq.
23.50	17000.00	7.665382	0.008759	287.4973	0.1953	Pb, liq.
23.50	18000.00	8.031079	0.011217	290.7358	0.2367	Pb, liq.
23.50	19000.00	8.430870	0.011508	294.6016	0.2473	Pb, liq.
23.50	20000.00	8.819532	0.009067	297.9767	0.2013	Pb, liq.
23.50	21000.00	9.249486	0.014700	302.0242	0.3059	Pb, liq.
23.50	22000.00	9.637950	0.021856	304.9350	0.4447	Pb, liq.
23.50	23000.00	10.081183	0.012460	308.8989	0.2601	Pb, liq.
23.50	24000.00	10.491432	0.018280	311.9396	0.3935	Pb, liq.
23.50	25000.00	10.954583	0.020738	315.8305	0.4058	Pb, liq.
23.50	26000.00	11.385390	0.022724	318.9958	0.4348	Pb, liq.
23.50	27000.00	11.863082	0.021520	322.8793	0.4096	Pb, liq.
23.50	28000.00	12.361370	0.020494	326.7929	0.4111	Pb, liq.
23.50	29000.00	12.824273	0.023357	330.0564	0.4726	Pb, liq.
23.50	30000.00	13.331946	0.020190	333.9911	0.3730	Pb, liq.
23.50	31000.00	13.739021	0.018793	335.6686	0.3464	Pb, liq.
23.50	32000.00	14.214167	0.025032	338.6296	0.4839	Pb, liq.
23.50	33000.00	14.762019	0.024041	342.6939	0.4621	Pb, liq.

continued ...

... continued

ρ (g/cm ³)	T (K)	E (eV/atom)	E_{error} (eV/atom)	P (GPa)	P_{error} (GPa)	note
23.50	34000.00	15.289450	0.030857	346.4947	0.5651	Pb, liq.
23.50	35000.00	15.781956	0.009450	348.9637	0.1623	Pb, liq.
23.50	36000.00	16.273090	0.038631	351.7942	0.6428	Pb, liq.
23.50	37000.00	16.923880	0.037706	357.0699	0.6964	Pb, liq.
23.50	38000.00	17.362780	0.039223	358.8745	0.7262	Pb, liq.
23.50	39000.00	17.994660	0.034341	363.4945	0.6068	Pb, liq.
23.50	40000.00	18.487140	0.035423	365.6236	0.6121	Pb, liq.
24.00	12000.00	6.252190	0.004265	286.0798	0.0969	Pb, liq.
24.00	13000.00	6.638542	0.007437	290.8181	0.1682	Pb, liq.
24.00	14000.00	6.978849	0.009991	294.3676	0.2224	Pb, liq.
24.00	15000.00	7.362684	0.013450	298.5988	0.2846	Pb, liq.
24.00	16000.00	7.703163	0.009122	301.7878	0.1938	Pb, liq.
24.00	17000.00	8.105230	0.008967	306.0561	0.2058	Pb, liq.
24.00	18000.00	8.477045	0.011451	309.4686	0.2499	Pb, liq.
24.00	19000.00	8.872989	0.012443	313.2179	0.2583	Pb, liq.
24.00	20000.00	9.262678	0.017026	316.7121	0.3609	Pb, liq.
24.00	21000.00	9.684660	0.010998	320.6182	0.2385	Pb, liq.
24.00	22000.00	10.096159	0.015757	324.0527	0.3334	Pb, liq.
24.00	23000.00	10.568438	0.015721	328.5545	0.3075	Pb, liq.
24.00	24000.00	10.953062	0.017337	331.1240	0.3506	Pb, liq.
24.00	25000.00	11.394550	0.022082	334.6163	0.4446	Pb, liq.
24.00	26000.00	11.867845	0.026151	338.5821	0.5265	Pb, liq.
24.00	27000.00	12.303087	0.028469	341.6719	0.5782	Pb, liq.
24.00	28000.00	12.735801	0.027137	344.4556	0.5263	Pb, liq.
24.00	29000.00	13.214548	0.026134	347.9928	0.5026	Pb, liq.
24.00	30000.00	13.724821	0.037978	351.9581	0.7332	Pb, liq.
24.00	31000.00	14.192517	0.029761	354.7900	0.5702	Pb, liq.
24.00	32000.00	14.723966	0.029439	358.8342	0.5753	Pb, liq.
24.00	33000.00	15.176981	0.021530	361.2086	0.3713	Pb, liq.
24.00	34000.00	15.754196	0.029879	365.7724	0.5656	Pb, liq.
24.00	35000.00	16.288647	0.017777	369.1717	0.3546	Pb, liq.
24.00	36000.00	16.733197	0.029029	371.1834	0.4948	Pb, liq.
24.00	37000.00	17.267725	0.036622	374.4690	0.6659	Pb, liq.
24.00	38000.00	17.875098	0.037422	378.8908	0.6571	Pb, liq.
24.00	39000.00	18.450022	0.040227	382.4296	0.6126	Pb, liq.
24.00	40000.00	19.070812	0.051382	386.8146	0.8438	Pb, liq.
24.50	12000.00	6.719278	0.007295	305.5160	0.1544	Pb, liq.
24.50	13000.00	7.092026	0.008428	310.0063	0.1912	Pb, liq.
24.50	14000.00	7.424676	0.010340	313.4049	0.2294	Pb, liq.
24.50	15000.00	7.812095	0.009309	317.8076	0.2108	Pb, liq.
24.50	16000.00	8.161333	0.009410	321.1600	0.2081	Pb, liq.
24.50	17000.00	8.565689	0.008074	325.4994	0.1758	Pb, liq.
24.50	18000.00	8.948216	0.010297	329.1919	0.2178	Pb, liq.
24.50	19000.00	9.356696	0.012924	333.2328	0.2675	Pb, liq.
24.50	20000.00	9.717373	0.010895	336.0399	0.2434	Pb, liq.
24.50	21000.00	10.123907	0.012856	339.6522	0.2742	Pb, liq.
24.50	22000.00	10.563665	0.014524	343.7016	0.3111	Pb, liq.
24.50	23000.00	10.977978	0.026835	347.0965	0.5430	Pb, liq.
24.50	24000.00	11.438500	0.018847	351.1038	0.4027	Pb, liq.
24.50	25000.00	11.864180	0.016290	354.3838	0.3367	Pb, liq.
24.50	26000.00	12.316150	0.017091	357.9906	0.3467	Pb, liq.
24.50	27000.00	12.803266	0.023266	362.0321	0.4734	Pb, liq.
24.50	28000.00	13.229098	0.033116	364.7328	0.6705	Pb, liq.
24.50	29000.00	13.744248	0.018943	368.9204	0.3439	Pb, liq.
24.50	30000.00	14.232734	0.033131	372.4987	0.6298	Pb, liq.
24.50	31000.00	14.658654	0.029925	374.6456	0.5526	Pb, liq.
24.50	32000.00	15.205203	0.032315	378.7812	0.6225	Pb, liq.
24.50	33000.00	15.653630	0.036436	381.0634	0.6804	Pb, liq.
24.50	34000.00	16.141745	0.033100	384.0961	0.6372	Pb, liq.
24.50	35000.00	16.735495	0.033580	388.8458	0.6250	Pb, liq.

continued ...

... continued

ρ (g/cm ³)	T (K)	E (eV/atom)	E_{error} (eV/atom)	P (GPa)	P_{error} (GPa)	note
24.50	36000.00	17.241169	0.028554	391.7941	0.5340	Pb, liq.
24.50	37000.00	17.793055	0.035598	395.2445	0.6415	Pb, liq.
24.50	38000.00	18.277036	0.036869	397.6534	0.6424	Pb, liq.
24.50	39000.00	18.825018	0.029831	401.0589	0.5223	Pb, liq.
24.50	40000.00	19.555848	0.048330	407.1940	0.8745	Pb, liq.
25.00	12000.00	7.190824	0.010384	325.6019	0.2310	Pb, liq.
25.00	13000.00	7.558091	0.007640	329.9873	0.1721	Pb, liq.
25.00	14000.00	7.908311	0.006665	333.7750	0.1580	Pb, liq.
25.00	15000.00	8.263016	0.008336	337.4595	0.1842	Pb, liq.
25.00	16000.00	8.646922	0.007200	341.6022	0.1623	Pb, liq.
25.00	17000.00	9.034660	0.010107	345.6267	0.2155	Pb, liq.
25.00	18000.00	9.426087	0.015190	349.5497	0.3210	Pb, liq.
25.00	19000.00	9.815375	0.013985	353.0994	0.2923	Pb, liq.
25.00	20000.00	10.248660	0.009609	357.5820	0.2045	Pb, liq.
25.00	21000.00	10.614297	0.017890	360.2937	0.3750	Pb, liq.
25.00	22000.00	11.050021	0.011951	364.2386	0.2612	Pb, liq.
25.00	23000.00	11.472756	0.016128	367.7255	0.3217	Pb, liq.
25.00	24000.00	11.922769	0.020282	371.6892	0.4373	Pb, liq.
25.00	25000.00	12.341566	0.022126	374.7731	0.4495	Pb, liq.
25.00	26000.00	12.807641	0.018845	378.6436	0.3810	Pb, liq.
25.00	27000.00	13.230108	0.017447	381.4993	0.3610	Pb, liq.
25.00	28000.00	13.716568	0.026682	385.2313	0.4699	Pb, liq.
25.00	29000.00	14.193074	0.021583	388.6847	0.4239	Pb, liq.
25.00	30000.00	14.695771	0.029721	392.7578	0.5822	Pb, liq.
25.00	31000.00	15.217316	0.025881	396.5626	0.4945	Pb, liq.
25.00	32000.00	15.673535	0.015284	399.1824	0.3091	Pb, liq.
25.00	33000.00	16.170282	0.034556	402.4882	0.5952	Pb, liq.
25.00	34000.00	16.719597	0.026103	406.5938	0.5091	Pb, liq.
25.00	35000.00	17.270099	0.045282	410.3401	0.7427	Pb, liq.
25.00	36000.00	17.749282	0.023478	412.7131	0.4413	Pb, liq.
25.00	37000.00	18.339882	0.039472	416.9052	0.6760	Pb, liq.
25.00	38000.00	18.865165	0.031569	419.8781	0.5475	Pb, liq.
25.00	39000.00	19.415630	0.029216	422.9778	0.4946	Pb, liq.
25.00	40000.00	19.937413	0.050677	426.1921	0.7729	Pb, liq.
13.50	12000.00	3.460350	0.009666	209.4937	0.2492	Sn, liq.
13.50	13000.00	3.783102	0.013804	213.1680	0.3498	Sn, liq.
13.50	14000.00	4.102613	0.019125	216.6174	0.4696	Sn, liq.
13.50	15000.00	4.493744	0.021180	221.6782	0.5389	Sn, liq.
13.50	16000.00	4.817294	0.019328	224.8442	0.4661	Sn, liq.
13.50	17000.00	5.209212	0.019538	229.5568	0.4929	Sn, liq.
13.50	18000.00	5.569239	0.015536	233.3277	0.3840	Sn, liq.
13.50	19000.00	5.952242	0.020897	237.3865	0.5110	Sn, liq.
13.50	20000.00	6.355108	0.024313	241.6333	0.5232	Sn, liq.
13.50	21000.00	6.736175	0.013541	245.5174	0.3389	Sn, liq.
13.50	22000.00	7.077196	0.022843	248.0733	0.5275	Sn, liq.
13.50	23000.00	7.494393	0.013946	252.3143	0.3367	Sn, liq.
13.50	24000.00	7.890887	0.013547	255.8942	0.3439	Sn, liq.
13.50	25000.00	8.310200	0.016070	259.8280	0.3939	Sn, liq.
13.50	26000.00	8.751966	0.023433	263.9896	0.5522	Sn, liq.
13.50	27000.00	9.208049	0.026346	268.4615	0.6288	Sn, liq.
13.50	28000.00	9.650739	0.023145	272.4538	0.5555	Sn, liq.
13.50	29000.00	10.067999	0.016308	275.7476	0.3744	Sn, liq.
13.50	30000.00	10.548077	0.011604	280.1976	0.2792	Sn, liq.
13.50	31000.00	11.009590	0.018451	284.1542	0.4378	Sn, liq.
13.50	32000.00	11.478493	0.029895	288.0640	0.6972	Sn, liq.
13.50	33000.00	11.935490	0.031608	291.5904	0.7116	Sn, liq.
13.50	34000.00	12.426584	0.037159	295.5728	0.8106	Sn, liq.
13.50	35000.00	12.964026	0.026347	300.5656	0.5936	Sn, liq.
13.50	36000.00	13.410489	0.025393	303.7318	0.5550	Sn, liq.
13.50	37000.00	13.956127	0.032009	308.5460	0.6923	Sn, liq.

continued ...

... continued

ρ (g/cm ³)	T (K)	E (eV/atom)	E_{error} (eV/atom)	P (GPa)	P_{error} (GPa)	note
13.50	38000.00	14.411554	0.034617	311.4180	0.7603	Sn, liq.
13.50	39000.00	14.942162	0.045336	315.4870	0.9486	Sn, liq.
13.50	40000.00	15.437769	0.055283	318.7876	1.1464	Sn, liq.
14.00	12000.00	4.004563	0.016634	234.7933	0.4267	Sn, liq.
14.00	13000.00	4.315310	0.013553	238.2860	0.3455	Sn, liq.
14.00	14000.00	4.695794	0.009232	243.4156	0.2558	Sn, liq.
14.00	15000.00	5.038390	0.013430	247.4103	0.3528	Sn, liq.
14.00	16000.00	5.407331	0.015364	251.8002	0.4016	Sn, liq.
14.00	17000.00	5.768437	0.018984	255.8251	0.4818	Sn, liq.
14.00	18000.00	6.078026	0.020213	258.4744	0.5064	Sn, liq.
14.00	19000.00	6.526024	0.015287	264.3012	0.3753	Sn, liq.
14.00	20000.00	6.902111	0.032592	268.3570	0.7962	Sn, liq.
14.00	21000.00	7.295322	0.024778	272.2794	0.6038	Sn, liq.
14.00	22000.00	7.722801	0.018860	277.1716	0.4876	Sn, liq.
14.00	23000.00	8.072746	0.022101	279.8514	0.5296	Sn, liq.
14.00	24000.00	8.528633	0.017606	284.9320	0.4117	Sn, liq.
14.00	25000.00	8.922798	0.025345	288.2389	0.5900	Sn, liq.
14.00	26000.00	9.341264	0.015144	292.3808	0.3643	Sn, liq.
14.00	27000.00	9.790005	0.020808	296.7193	0.5121	Sn, liq.
14.00	28000.00	10.212521	0.020145	300.2945	0.4806	Sn, liq.
14.00	29000.00	10.678831	0.013619	304.8531	0.2950	Sn, liq.
14.00	30000.00	11.133687	0.025237	308.9744	0.5331	Sn, liq.
14.00	31000.00	11.559503	0.019524	311.8089	0.4861	Sn, liq.
14.00	32000.00	12.041797	0.024809	316.3565	0.5625	Sn, liq.
14.00	33000.00	12.481815	0.017466	319.6708	0.3794	Sn, liq.
14.00	34000.00	13.042225	0.025816	325.6239	0.5487	Sn, liq.
14.00	35000.00	13.490160	0.026697	328.8127	0.5942	Sn, liq.
14.00	36000.00	13.976973	0.023784	332.5400	0.5074	Sn, liq.
14.00	37000.00	14.470441	0.045255	336.5893	1.0513	Sn, liq.
14.00	38000.00	15.013894	0.031595	341.2415	0.7168	Sn, liq.
14.00	39000.00	15.461843	0.063489	344.0139	1.4318	Sn, liq.
14.00	40000.00	16.045896	0.042029	349.8404	0.9842	Sn, liq.
14.50	12000.00	4.582912	0.007015	262.1011	0.1886	Sn, liq.
14.50	13000.00	4.937393	0.017456	266.8270	0.4647	Sn, liq.
14.50	14000.00	5.292630	0.011201	271.4652	0.2945	Sn, liq.
14.50	15000.00	5.645561	0.009642	275.8260	0.2559	Sn, liq.
14.50	16000.00	6.016510	0.014799	280.4525	0.3866	Sn, liq.
14.50	17000.00	6.316768	0.021216	283.0690	0.5591	Sn, liq.
14.50	18000.00	6.730226	0.014224	288.4337	0.3641	Sn, liq.
14.50	19000.00	7.132308	0.020820	293.2898	0.5243	Sn, liq.
14.50	20000.00	7.536297	0.013867	297.9617	0.3677	Sn, liq.
14.50	21000.00	7.933773	0.021921	302.2864	0.5628	Sn, liq.
14.50	22000.00	8.335195	0.019873	306.5897	0.5011	Sn, liq.
14.50	23000.00	8.683242	0.013042	309.3775	0.3075	Sn, liq.
14.50	24000.00	9.102184	0.012355	313.5723	0.3428	Sn, liq.
14.50	25000.00	9.565255	0.021404	319.0003	0.5468	Sn, liq.
14.50	26000.00	9.964053	0.015277	322.4767	0.3925	Sn, liq.
14.50	27000.00	10.408139	0.019740	326.8830	0.4950	Sn, liq.
14.50	28000.00	10.840036	0.017365	330.8232	0.4325	Sn, liq.
14.50	29000.00	11.218068	0.027258	333.4370	0.6788	Sn, liq.
14.50	30000.00	11.720276	0.030036	338.5723	0.7006	Sn, liq.
14.50	31000.00	12.165622	0.043037	342.4442	1.0157	Sn, liq.
14.50	32000.00	12.667698	0.023781	347.5370	0.5507	Sn, liq.
14.50	33000.00	13.082951	0.026961	350.2787	0.6444	Sn, liq.
14.50	34000.00	13.559696	0.035368	354.6054	0.8685	Sn, liq.
14.50	35000.00	14.096980	0.028031	359.5290	0.7128	Sn, liq.
14.50	36000.00	14.589731	0.044928	363.9389	1.0866	Sn, liq.
14.50	37000.00	15.048731	0.032162	367.2713	0.7033	Sn, liq.
14.50	38000.00	15.550744	0.035261	371.2555	0.7974	Sn, liq.
14.50	39000.00	16.084960	0.059644	375.9744	1.3244	Sn, liq.

continued ...

... continued

ρ (g/cm ³)	T (K)	E (eV/atom)	E_{error} (eV/atom)	P (GPa)	P_{error} (GPa)	note
14.50	40000.00	16.654874	0.033684	381.2377	0.7290	Sn, liq.
15.00	12000.00	5.239390	0.013665	292.6380	0.3456	Sn, liq.
15.00	13000.00	5.556495	0.011242	296.5354	0.3298	Sn, liq.
15.00	14000.00	5.930396	0.017716	301.7407	0.4907	Sn, liq.
15.00	15000.00	6.284514	0.017718	306.2174	0.4901	Sn, liq.
15.00	16000.00	6.602185	0.013503	309.5318	0.3505	Sn, liq.
15.00	17000.00	7.029032	0.014551	315.5346	0.3659	Sn, liq.
15.00	18000.00	7.357669	0.020777	318.9022	0.5440	Sn, liq.
15.00	19000.00	7.719538	0.026584	322.8074	0.6786	Sn, liq.
15.00	20000.00	8.196538	0.026469	329.5572	0.6880	Sn, liq.
15.00	21000.00	8.578672	0.027176	333.7037	0.7112	Sn, liq.
15.00	22000.00	8.933430	0.029838	336.8847	0.7391	Sn, liq.
15.00	23000.00	9.310148	0.020309	340.2428	0.5301	Sn, liq.
15.00	24000.00	9.753736	0.012579	345.4284	0.3228	Sn, liq.
15.00	25000.00	10.163655	0.016098	349.5021	0.4071	Sn, liq.
15.00	26000.00	10.561555	0.016104	353.2210	0.3813	Sn, liq.
15.00	27000.00	11.014396	0.019411	358.0155	0.4858	Sn, liq.
15.00	28000.00	11.416771	0.023859	361.2947	0.6106	Sn, liq.
15.00	29000.00	11.935960	0.018195	367.3782	0.4574	Sn, liq.
15.00	30000.00	12.363566	0.025636	371.0630	0.6492	Sn, liq.
15.00	31000.00	12.866755	0.028633	376.3065	0.7265	Sn, liq.
15.00	32000.00	13.375874	0.033752	381.5801	0.7584	Sn, liq.
15.00	33000.00	13.796051	0.018316	384.6439	0.4619	Sn, liq.
15.00	34000.00	14.271286	0.032851	388.7398	0.8052	Sn, liq.
15.00	35000.00	14.765281	0.034918	393.2080	0.7936	Sn, liq.
15.00	36000.00	15.254775	0.030343	397.6500	0.6816	Sn, liq.
15.00	37000.00	15.759093	0.025198	401.7864	0.6278	Sn, liq.
15.00	38000.00	16.203336	0.034807	404.8564	0.7483	Sn, liq.
15.00	39000.00	16.709119	0.045350	409.0046	1.0015	Sn, liq.
15.00	40000.00	17.300742	0.039786	414.9578	0.9597	Sn, liq.
15.50	12000.00	5.890876	0.017640	324.3202	0.4860	Sn, liq.
15.50	13000.00	6.260765	0.015980	329.7561	0.4508	Sn, liq.
15.50	14000.00	6.601620	0.012750	334.1011	0.3351	Sn, liq.
15.50	15000.00	6.944910	0.014567	338.4469	0.4078	Sn, liq.
15.50	16000.00	7.301528	0.017838	342.8766	0.4839	Sn, liq.
15.50	17000.00	7.674644	0.020470	347.7438	0.5463	Sn, liq.
15.50	18000.00	8.068483	0.018058	352.7632	0.4734	Sn, liq.
15.50	19000.00	8.435599	0.029300	356.8992	0.7607	Sn, liq.
15.50	20000.00	8.818009	0.026390	361.2162	0.6961	Sn, liq.
15.50	21000.00	9.246835	0.031620	366.7504	0.8375	Sn, liq.
15.50	22000.00	9.574811	0.016744	369.4487	0.4245	Sn, liq.
15.50	23000.00	9.987841	0.015967	373.9510	0.4373	Sn, liq.
15.50	24000.00	10.404700	0.024327	378.5726	0.6227	Sn, liq.
15.50	25000.00	10.878299	0.017398	384.3097	0.4459	Sn, liq.
15.50	26000.00	11.273211	0.019309	387.8429	0.5054	Sn, liq.
15.50	27000.00	11.671612	0.016268	391.3259	0.4385	Sn, liq.
15.50	28000.00	12.172118	0.016902	397.3977	0.4386	Sn, liq.
15.50	29000.00	12.578995	0.023057	400.6931	0.5580	Sn, liq.
15.50	30000.00	13.036629	0.035681	405.4156	0.8883	Sn, liq.
15.50	31000.00	13.473088	0.021304	409.0829	0.5305	Sn, liq.
15.50	32000.00	13.929220	0.035625	413.3568	0.8695	Sn, liq.
15.50	33000.00	14.502850	0.032632	420.0162	0.8089	Sn, liq.
15.50	34000.00	14.881349	0.030835	422.1764	0.7365	Sn, liq.
15.50	35000.00	15.452971	0.039165	428.6627	0.9305	Sn, liq.
15.50	36000.00	15.919972	0.030601	432.0734	0.7162	Sn, liq.
15.50	37000.00	16.398823	0.046140	435.9163	1.0870	Sn, liq.
15.50	38000.00	16.936166	0.041490	441.3354	0.9635	Sn, liq.
15.50	39000.00	17.417838	0.038525	445.2359	0.9009	Sn, liq.
15.50	40000.00	17.856602	0.053280	447.3523	1.2051	Sn, liq.
16.00	12000.00	6.588552	0.010326	358.5386	0.2844	Sn, liq.

continued ...

... continued

ρ (g/cm ³)	T (K)	E (eV/atom)	E_{error} (eV/atom)	P (GPa)	P_{error} (GPa)	note
16.00	13000.00	6.963115	0.008863	364.2064	0.2645	Sn, liq.
16.00	14000.00	7.296499	0.011164	368.5440	0.3202	Sn, liq.
16.00	15000.00	7.667942	0.012257	373.7580	0.3362	Sn, liq.
16.00	16000.00	7.986862	0.023726	377.2274	0.6304	Sn, liq.
16.00	17000.00	8.387534	0.011216	382.9230	0.2994	Sn, liq.
16.00	18000.00	8.784691	0.018839	388.1555	0.5334	Sn, liq.
16.00	19000.00	9.127327	0.021727	391.6908	0.5879	Sn, liq.
16.00	20000.00	9.533076	0.020942	396.7413	0.5673	Sn, liq.
16.00	21000.00	9.933283	0.024231	401.6466	0.6539	Sn, liq.
16.00	22000.00	10.334831	0.024931	406.1694	0.5965	Sn, liq.
16.00	23000.00	10.720260	0.018324	410.1779	0.4803	Sn, liq.
16.00	24000.00	11.176589	0.014799	415.8585	0.3876	Sn, liq.
16.00	25000.00	11.556170	0.016564	419.4221	0.4253	Sn, liq.
16.00	26000.00	11.969329	0.019789	423.5549	0.5300	Sn, liq.
16.00	27000.00	12.386591	0.016447	427.6021	0.4415	Sn, liq.
16.00	28000.00	12.822914	0.020080	431.9745	0.5029	Sn, liq.
16.00	29000.00	13.382687	0.021465	439.2861	0.5656	Sn, liq.
16.00	30000.00	13.718886	0.020638	441.0250	0.5136	Sn, liq.
16.00	31000.00	14.243119	0.018333	447.2015	0.4761	Sn, liq.
16.00	32000.00	14.708282	0.037634	451.6111	0.9578	Sn, liq.
16.00	33000.00	15.212158	0.030973	456.7367	0.7536	Sn, liq.
16.00	34000.00	15.622535	0.032029	459.6234	0.7620	Sn, liq.
16.00	35000.00	16.115131	0.031839	464.3711	0.8149	Sn, liq.
16.00	36000.00	16.555052	0.020730	467.7551	0.4639	Sn, liq.
16.00	37000.00	17.138811	0.032858	474.1377	0.8112	Sn, liq.
16.00	38000.00	17.546811	0.037717	476.1300	0.9359	Sn, liq.
16.00	39000.00	18.094883	0.029588	481.5681	0.7611	Sn, liq.
16.00	40000.00	18.686321	0.048779	488.1845	1.0903	Sn, liq.
12.50	5000.00	-4.980080	0.002119	247.1710	0.0645	Fe, sol.
13.50	5000.00	-4.181941	0.001539	337.7488	0.0441	Fe, sol.
13.00	5000.00	-1.083734	0.002473	186.3594	0.1085	Cu, sol.
13.00	6000.00	-0.760377	0.003942	195.4087	0.1721	Cu, sol.
13.50	5000.00	-0.793778	0.001635	216.3550	0.0776	Cu, sol.
13.50	6000.00	-0.477312	0.003917	225.4728	0.1695	Cu, sol.
14.00	5000.00	-0.467014	0.001887	249.6611	0.0901	Cu, sol.
14.00	6000.00	-0.143542	0.005534	259.3500	0.2615	Cu, sol.
14.50	5000.00	-0.108334	0.002295	286.0529	0.0963	Cu, sol.
14.50	6000.00	0.204252	0.002030	295.5932	0.0933	Cu, sol.
14.50	7000.00	0.532781	0.005487	305.4198	0.2508	Cu, sol.
15.00	5000.00	0.280577	0.000841	325.6906	0.0538	Cu, sol.
15.00	6000.00	0.590610	0.001362	335.3652	0.0681	Cu, sol.
15.00	7000.00	0.917560	0.003443	345.4495	0.1676	Cu, sol.
12.00	5000.00	-5.302303	0.003458	208.0766	0.1526	Fe, sol*
13.00	5000.00	-4.607604	0.002558	290.3764	0.0785	Fe, sol*
13.00	6000.00	-4.162117	0.021780	303.7985	0.8596	Fe, sol*
13.50	6000.00	-3.782597	0.002581	349.4452	0.0848	Fe, sol*
13.50	7000.00	-0.088877	0.024718	237.4735	1.1242	Cu, sol*